www.vbripress.com/aml, DOI: 10.5185/amlett.2016.6384 Published online by the VBRI Press in 2016

Synthesis and doping feasibility of composite-hydroxide-mediated approach for the $Cu_{1-x}Zn_xO$ nanomaterials

Tauseef Shahid[1], Muhammad Arfan[1], Waqas Ahmad[1], Tayyaba BiBi[4,5], Taj Muhammad Khan[2,3*]

[1]*Department of Applied Physics, Federal Urdu University of Arts, Science and Technology, Islamabad 44000, Pakistan*
[2]*National Institute of Lasers and Optronics (NILOP), Islamabad 44000, Pakistan*
[3]*School of Physics, Trinity College Dublin (TCD), Dublin 2, Ireland*
[4]*Peshawar University, Department of Chemistry, Peshawar 45000, Pakistan*
[5]*Dublin Institute of Technology (DIT), Dublin 8, Ireland*

[*]Corresponding author. Tel: (+92) 51-9248801; Fax: (+92) 51-2208051; E-mail: tajakashne@gmail.com

Received: 24 December 2015, Revised: 09 February 2016 and Accepted: 22 May 2016

ABSTRACT

In this article, we report feasibility of composite hydroxide-mediated (CHM) approach for the synthesis and doping of Cu1-xZnxO (x=0%, 3%, 6% and 9%) nanomaterial. The proposed method offers a low cost, low temperature and environmentally friendly approach to preparing doped nanomaterials in a feasible and cost- effective route. Further, we investigate the effect of incorporated Zn^{+2} on the properties of produced Cu (II) O nanostructures. The X-ray diffraction analysis confirms formation of the single-phase monoclinic Cu (II) O and incorporation of Zn at the Cu-lattice sites. The crystalline structure is improved and the average grain size has increased from 85.32 nm to 124.86 nm. FTIR spectroscopy shows characteristic vibrational peaks of the Cu (II)-O bonding which confirms formation of the Cu (II) O. SEM micrographs reveal interesting flower like dense features with morphological peculiarities and seems to strongly depend on the content of the incorporated Zn^{+2}. The UV- visible spectra are measured to study the direct bandgap of the prepared nanomaterial. The direct bandgap found to be in the range of 3.73 - 3.89 eV. The method seems experimentally friendly and provides a feasible and a high productive fast synthesis route for the doped oxide nanomaterials in a single step with tunable properties for the research purposes. However, the method still requires further investigation to finely control doping for the desired properties of a nanomaterial and to give a potential avenue for further practical scale-up of the production process and applications of novel devices based on doped nanostructures.

Keywords: $Cu_{1-x}Zn_xO$; nanomaterials; SEM; CHM; bandgap.

Introduction

Semiconductor oxide nanomaterials have received considerable attention due to their attractive chemical and physical properties which are different from their bulk counterparts. These nanomaterials have interesting optical, electronic and photocatalytic properties due to the quantum size effect **[1]**. Recently, extensive efforts have been paid to synthesize nanostructures of transition metal-oxides including; ZnO, CdO, PdO, CuO etc., and to explain their physical and chemical properties because of their potential applications in various sectors of technological importance. Among these semiconductor oxide nanomaterials, CuO is an important p-type semiconductor with a narrow band gap of 1.2 eV and monoclinic phase structure **[2, 3]**. CuO is a distinguishable and versatile candidate for potential applications in various fields such as gas sensors, catalyst, thermo electronic materials, biosensors, field emission devices, high temperature superconductors, photovoltaic devices, energy storage and spintronics **[4-12]**. Various physical and chemical techniques have been applied for the synthesis of CuO nanomaterials including; colloid-thermal, alcohol-thermal, sonochemical method, sol-gel, hydrothermal, reverse micelles, solid state reaction, solvothermal, thermal oxidation and milling **[13-22]** etc. Although these methods are used for the preparation of nanomaterials but still there are some limitations making them less feasible and environmentally non friendly. Some of these are low cost but require high annealing temperature as a final step; while some of them are practical methods to synthesize nanostructures of many kinds but they require surfactants and organic solvents and seems to be not truly environmentally friendly green methods. These methods have their own advantages and disadvantages but a green synthesis approach should have three essential components like eco-friendly reducing and capping reagents and acceptable solvent system. A technique used for the preparation of nanomaterials which seems truly a green and feasible synthesis route is the composite-hydroxide-mediated (CHM) approach. This approach requires no vacuum and a high temperature, high pressure, or low temperature with high pressure. It is based on a single step process requires no annealing or grinding and is a template free methodology. So for CHM approach has been used for the preparation of a wide range of nanostructures including; complex oxides, hydroxides, simple metal oxides, sulfides,

selenides, tellurides, fluorides and metals. Using this method, synthesis and doping of the nanomaterials can be carried out in a single step process more efficiently. The method can be applied for the synthesis of various doped nanomaterials in a cost effective and feasible way with large potential for practical applications. Nanomaterials doping by CHM seems to depend strongly on the synthesis temperature and processing time of the chemicals and is under investigation in research direction. Recently, Khan et al. used this method for the preparation of ZnO (nanoawires, nanorods) and CdO nanoparticles and investigated the effect of synthesis temperature on the morphology and particle size of the produced nanomaterials **[23, 24]**. Recently, this method has extended to the preparation of complex structured nanomaterials **[25]**. In fact, this method enjoys the advantages with the synthesis of functional wires, rods, belts and other various nanostructures. The method is economically suitable and has used to synthesize CuO with controlled synthesis temperature and with different morphology of the nanostructures for research purposes **[25, 26]**. Recently this method was used for transition metal doping in multifunctional nanomaterials and interesting results were produced. Enhanced room temperature ferromagnetic property and a shift in the absorption peak from ultraviolet region to visible light region was observed for the Mn doped CeO_2 **[27]**. However, the method is still under extensive investigation in research direction for various elemental doping in semiconductor oxides with controlled morphology, particle size and crystallinity for research purposes. Previously, a number of researchers have performed transition metal doping in CuO by different methods but only a few of these works are about Zn doped CuO nanomaterials. Moreover, related studies to the Zn doping by CHM approach is still demanding for realization in practical applications.

This report describes the feasibility of CHM approach for the synthesis of Zn doped CuO nanostructures at constant temperature (200 ^oC) and constant processing time (24 h). The method seems to be a novel approach to present a simple and cost effective route for the direct elemental doping in nanomaterials during the synthesis process for research purposes. The key point of this method is to prepare and doped nanomaterials at the same time in single step process in a feasible way. This study further includes investigation on the effects of Zn^{+2} doping on the structural, morphological and optical properties of the CuO nanomaterial. Appropriate mechanisms of the formation of CuO by CHM are proposed.

Experimental

Materials and methods

All the chemical materials used for the synthesis were analytical grade chemicals and used without any further purification. They were obtained from E-Merck Co. with quoted purity 99.99 %. The chemicals used were $Cu(NO_3)_2.3H_2O$, $Zn(NO_3)_2.3H_2O$, NaOH and KOH.

Experimental procedure for the synthesis of nanomaterials using CHM is given in our previous reports **[23, 24]**. Briefly, a 10 g of mixed hydroxides (NaOH: KOH=51.5:48.5) was taken in a Teflon vessel and heated up to 200 ^oC in a preheated furnace for 24 hours. When the hydroxides were totally molten, an amount of 2.5 g of $Cu(NO_3)_2.3H_2O$ was added and the mixture was stirred until a uniform blue precursor was obtained. After 24h, the vessel was taken out and let it cool down to room temperature through natural cooling. This procedure was also done for Zn doped CuO nanostructures where $Zn(NO_3)_2.3H_2O$ was added in the quantities as (3%, 6% and 9%). A certain amount of blue precursor was dissolved in various volumes of deionized water. After aging for several hours, the product was filtered and washed thoroughly by deionized water to remove residual hydroxides. The washed crystals were dried at 40 ^oC for 24 hrs. **Fig. 1** shows a general sketch of the CHM approach demonstrating various steps involved in the synthesis of CuO.

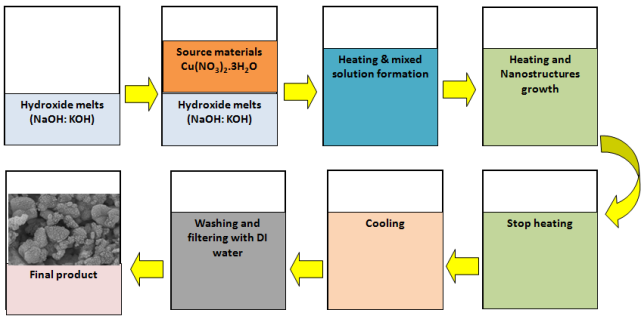

Fig. 1. Illustration of the various steps of CHM approach involved in the synthesis of CuO nanomaterial.

The chemical reactions representing formation of Zn doped CuO nanocrystals are as follows;

$$Cu(NO_3)_2.3H_2O + 2NaOH \rightarrow Cu(OH)_2 + 2NaNO_3 + 3H_2O$$

The product $Cu(OH)_2$ is chemically not stable at higher temperatures to forms CuO nanostructures and precipitates as;

$$Cu(OH)_2 \rightarrow CuO + H_2O$$

NaOH and KOH are high melting point melts but CHM approach basically involves the chemical reactions in eutectic hydroxides melts at a temperature approximately of 200 ^oC. These hydroxides are used as an important reaction medium at reduced the reaction temperature of the reactants for the preparation of nanomaterials. The obtained product is a pure polycrystalline nanomaterial to use for further characterization and investigation.

Characterization methods

Structural analysis was done by using XRD PANalytical model X'pert PRO Origin X-ray diffractometer operated at 40 kV and 30 mA using CuKα monochromatic radiation (λ =1.5406 Å). Scanning electron microscopy (SEM) was employed for the analysis of microstructures and surface morphology. A Fourier transform infrared interferometer (PMQ II, Carl Zeiss) was used to measure transmittance in spectral range of interest (400-4000 cm^{-1}). The UV-visible absorption spectroscopy was carried out in the spectral range of 200-800 nm. Optical band gap was estimated from the absorption data of the UV-visible spectra for all the prepared samples.

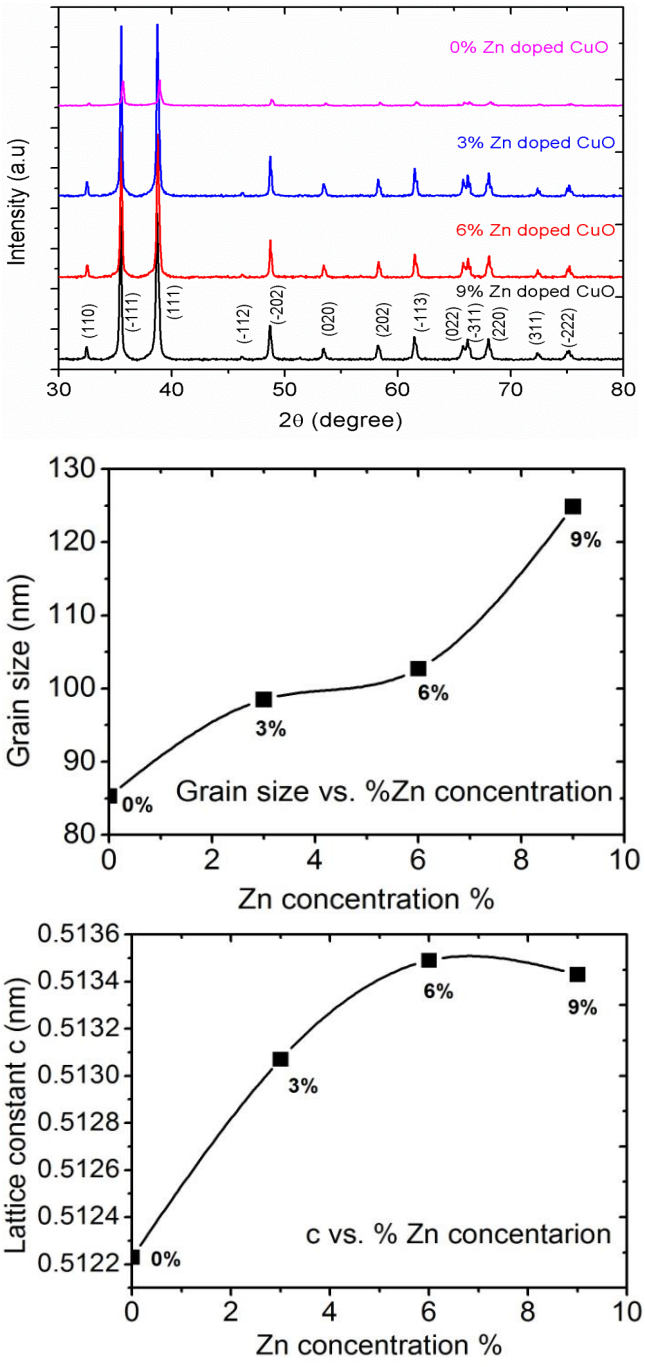

Fig. 2. X-ray diffraction pattern of Zn doped CuO nanomaterial ($Cu_{1-x}Zn_xO$, x = 0%, 3%, 6% and 9%) prepared at 200°C for 24 h. Variation of the grain size (*D* nm) and lattice constant (*c* nm) with Zn concentration is also shown in the same figure.

Results and discussion

XRD analysis

The XRD patterns of all the samples show diffraction peaks observed at 2θ values from 20-80° with a step size of 0.04° (**Fig. 2**). The peaks are observed for (110), (-111), (111), (-112), (-202), (020), (202), (-113), (022), (-311), (220), (311), (-222) planes. The observed sharp diffraction peaks clearly demonstrate a single phase polycrystalline CuO with a monoclinic structure. The XRD pattern obtained is closely matched with the reference pattern of CuO (ICDD.PDF2 00-005-0661). The strong intensities of (-111) and (111) peaks reveal that mostly crystallites are oriented in these planes directions. The peak intensity and position gives a strong evidence on the formation of Zn doped CuO because the peak intensity is determined by the nature of the atom and perhaps the available atoms in a diffraction plane. Similarly, if the associated atoms in a diffracting plane of a unit cell are different or if the atoms in a particular plane are strained or compressed (depends on the size of the dopant atom) due to the dopant foreign impurity atom, the reflection intensity will be different for that particular plane. Another possible reason for the higher peak intensities due to (-111) and (111) planes may be due to difference in the surface free energies (G) for the main crystallographic planes of the monoclinic CuO. Due to this anisotropy, preferential growth on the plane of lowest energy occurs and is accounted for the observed larger intensity of the diffraction peaks in the XRD pattern **[28]**. These peaks are used to calculate the d-spacing using Bragg's equation (d = nλ/2Sinθ) **[29]**.

Table 1. Calculated structural and optical parameters of $Cu_{1-X}Zn_XO$ in comparison with standard parameters of Cu (II) O

X (%)	a (nm)	b (nm)	c (nm)	d (nm)	cell volume $(nm)^3$	Grain size (D) (nm)	E_g (eV)
0.0	0.46778	0.34175	0.51223	0.2 3287	80.77	85.32	3.76
3.0	0.46930	0.34274	0.51307	0.23179	81.38	98.50	3.89
6.0	0.46880	0.34254	0.51349	0.23 16 8	81.31	102.71	3.73
9.0	0.46898	0.34251	0.51343	0.23 157	81.33	124.86	3.77
*	0.46840	0.34250	0.51220	0.2 3118	81.16	- - - -	1.2

* Standard literature values **[37]**.

The calculated values for these (-111) and (111) prominent planes are; 0.25165 nm and 0.23287 nm respectively. In the XRD pattern no impurity peaks related to Zn or its related compounds are observed. This means formation of pure CuO or the Zn phases are very small and disappeared in the noise signals. Furthermore, the diffraction peaks in the doped samples are low angle shifted compared to pure sample. This gives a strong signature on the fact that Zn has been incorporated at the Cu-lattice sites in the crystal structure.

The average grain sizes (*D*) of the nanocrystal is calculated by using Debye-Scherrer's formula **[30]**;

$$D = 0.94\lambda / \beta\cos\theta \quad (1)$$

where, λ is the radiation wavelength in nm, β is the full width at half maximum (FWHM) of a diffraction peak in radian units, θ_B is the diffraction angle and 0.94 is the Scherrer constant. The average grain size increases from 82.32 nm to 124.86 nm with Zn concentration. The calculated lattice parameters and average grain size are listed in **Table 1**. The modification in the lattice constants and d spacing values can be associated with the induced changes caused by Zn doping. Other possible native imperfections due to morphological changes and oxygen vacancies can also lead to such variation in the lattice constants and *d*-spacing. Moreover, as the particle size increases, the unit cell volume and micro-strain decrease which would result in to modify the lattice constants and *d*-spacing values. The variation in lattice constant (*c*) and

grain size (*D*) with Zn concentration are also shown in the same **Fig. 2**.

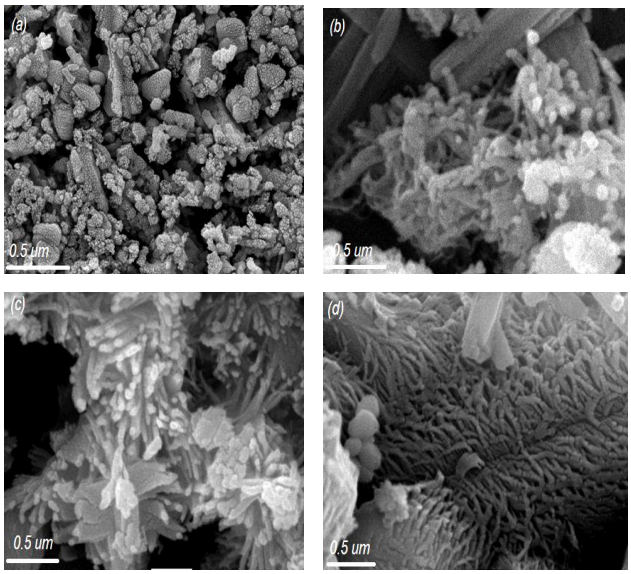

Fig. 3. SEM micrographs of the Zn doped CuO nanostructures ($Cu_{1-x}Zn_xO$) a) x = 0%, b) 3%, c) 6% and d) %) prepared at 200°C for 24 h.

Scanning electron microscopy (SEM) study

Microstructure and morphology of the prepared $Cu_{1-x}Zn_xO$ (x=0%, 3%, 6%, 9%) nanomaterial is analyzed with scanning electron microscopy and SEM micrographs at resolution of X 10, 000 are illustrated in **Fig. 3 (a-d)** respectively**.** These typical low magnification SEM images show interesting peony and dahlia- flowers type dense nanostructures. The morphologies of the nanostructures change and seem strongly to depend on the Zn concentration. Some of these consist of dense lace flower like structures with thickness of about 10-40 nm and size of a single flower is about 2.5 um. The microstructures are connected together on the bases, rooted in one centre and present a beautiful flower like morphology. The pure CuO sample has random orientation and non-uniform distribution; while the Zinc doped CuO prepared at the same conditions have flower like structure which can be clearly seen in the SEM micrographs. An interesting mixed morphological structure is formed as the concentration of Zn was increased to 6%. The formation mechanisms of CuO nanomaterial is based on the higher concentration of OH^- ions in the growth solution and viscosity of the melts at the processing temperature. Both the hydroxide ions and viscosity of the melts favor to speed up formation process of CuO peony-flower nanostructures due to larger number of growth nuclei sites. At the beginning only a few CuO nuclei are produced however, as the growth process progresses, surfaces of the produced CuO nuclei either gets a negative or a positive charge. The produced opposite charges (OH^- and Cu^{+2}) attract each other to form $Cu(OH)_2$ which further is decomposed into CuO and water molecule. The effect of kinematic viscosity of the melts on the formation of CuO nanomaterial by CHM is still poorly understood due to the involved complex thermodynamics. However, it is noteworthy to mention here that a higher viscosity medium reduces the speed of nucleation, aggregation and recrystallization and results in the formation of bigger crystallites in the final nanoproduct.

FTIR analysis

FTIR is conducted on the prepared samples in the region of 400-4000 cm^{-1} however the displayed spectra show a frequency range of our interest of 200 -1600 cm^{-1}. This characterization is carried out in order to understand the chemical and structural roots of the prepared nanostructures of CuO with the effects of reaction materials used to synthesize pure and doped CuO. FTIR spectra of (0%, 3%, 6% and 9%) Zn doped CuO nanomaterial is given in **Fig. 4.** All the samples show characteristics vibrational modes of monoclinic CuO according to literature **[31]**. For the CuO nanostructures the two main vibrational modes are observed in the frequencies ranges of 472 - 482 and 577 - 588 cm^{-1}. The high frequency mode at 584-588 cm^{-1} is reported due to Cu-O vibration along [101] direction. Furthermore, the peaks are observed for the samples with 3% doped Zn is 588 cm^{-1}, 6% Zn doped are 584 and 474 cm^{-1} and 9% Zn doped is 577 cm^{-1} attributed to vibrational modes of CuO monoclinic structure **[31]**. This strongly supports the results obtained with XRD shows the formation of a pure and single phase CuO nanomaterial.

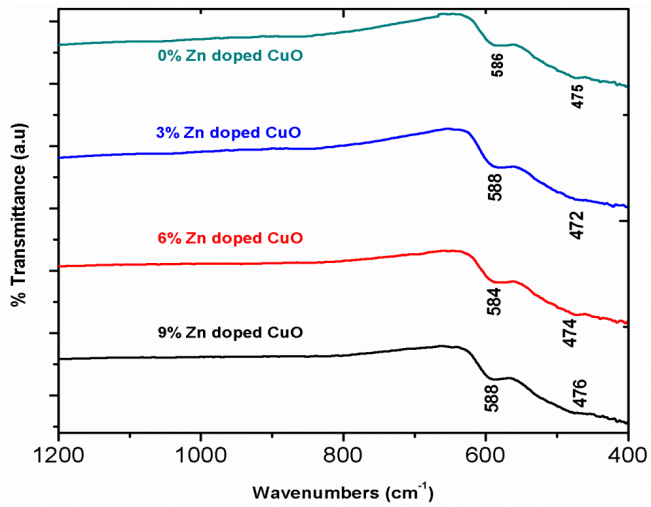

Fig. 4. FT-IR spectra of the Zn doped CuO nanostructures ($Cu_{1-x}Zn_xO$, x = 0%, 3%, 6% and 9%) prepared by CHM approach at constant temperature (200°C) and constant reaction time (24 h).

UV-visible spectroscopy

UV-visible is conducted on the samples to investigate the optical behavior of the prepared nanomaterial and to evaluate the optical bandgap to see the doping effect. The UV-visible absorption spectra, bandgap and variation in bandgap of CuO pure with Zn plots for the pure and Zn doped CuO Nanomaterials are displayed in **Fig. 5 (a-c)** respectively**.** Before measurements, pure and Zn doped CuO nanomaterial is dispersed in methanol by ultrasonic vibration for 15 minutes. The strong and sharp absorption peaks are observed for the samples with Zn concentration of 3%, 6% and 9% at 202, 204, 209 nm, respectively which are associated with quartz cuvette **[32]**.

The UV-visible spectra exhibit weak absorption peaks centered at about 372 and 381 nm are attributed to the bandgap transition of Cu (II) O **[33]**. The peaks at 650 to 800 nm are attributed due to the presence of CuO nanostructures at the surface **[34]**.

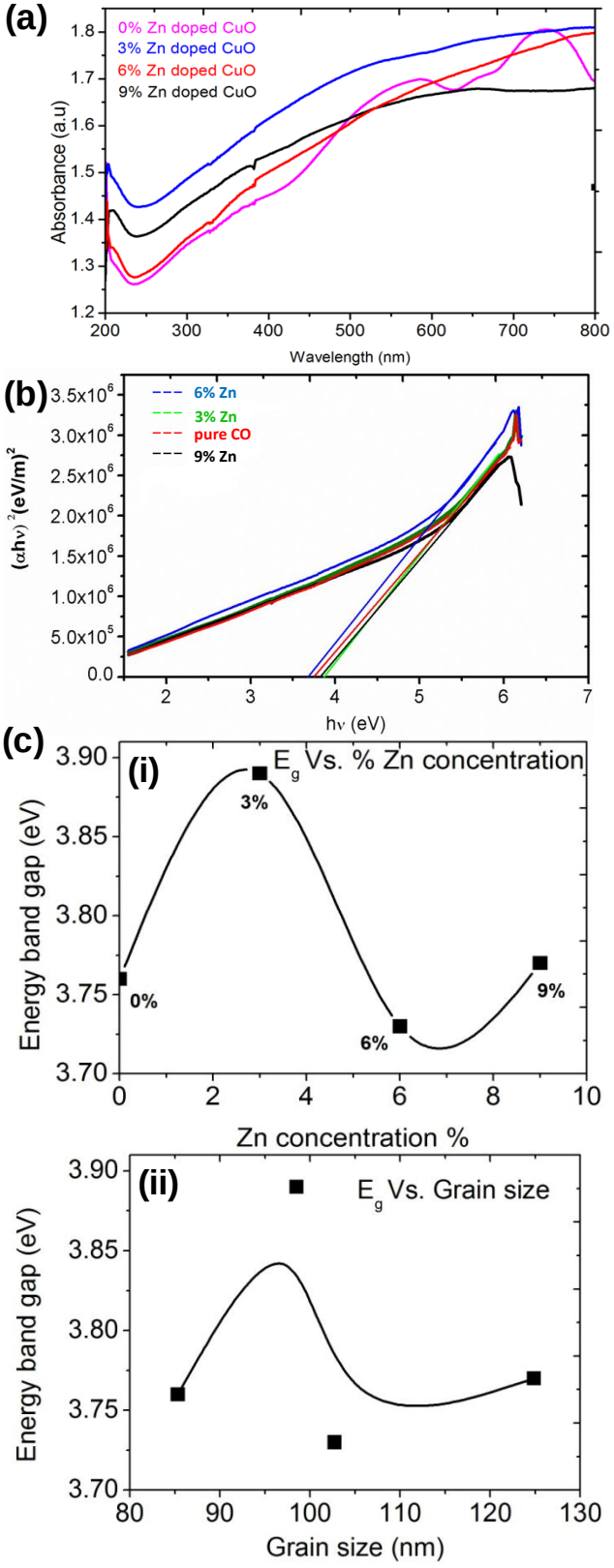

Fig. 5. (a) UV-vis. absorption spectra of the Zn doped CuO nanostructures for various Zn concentrations; 0 %, 3 %, 6 %, and 9 % prepared by CHM method at 200°C, (b) The $(\alpha h\upsilon)^2$ vs. hυ plot of pure and Zn doped CuO. E_g is the intercept of the line at hν-axis for the bandgap calculation and (c) Variation of the direct bandgap with (i) Zn concentration and (ii) grain size.

The comparative figure reveals that absorption has increased for the Zn concentration of 3% and 6% sample; while absorption drops a little for the sample with 9% Zn. The absorption spectra clearly indicate that the samples show absorbance for entire UV-visible region. This suggests that these nanostructures are best to utilize for the solar cell application. The absorption spectrum is used to determine energy band gap of the prepared CuO by well-known Tauc's formula **[35]**;

$$\alpha h\upsilon = B\,(h\upsilon - Eg)^n \qquad (2)$$

here, h is the plank's constant, υ is frequency of the photon; hν is photon energy in eV, E_g is optical band gap in eV, B is a constant, n is an exponent which is 2 for indirect band transitions and 1/2 for direct band transition and α is the absorption coefficient calculated by using the formula;

$$\alpha = 2.303 * {}^{A}/_{l} \qquad (3)$$

where, A is known as absorbance and ℓ is known as the path length of quartz cuvette. **Fig. 5 (b)** shows the plot $(\alpha h\upsilon)^2$ vs. hυ of pure and Zn doped CuO. The direct band gap energy for the samples can be estimated by extrapolating the linear region of $(\alpha h\upsilon)^2$ vs. hυ to the point α = 0. Thus the E_g is the intercept of the line at hν-axis. The obtained direct band gap values are 3.76, 3.89, 3.73 eV and 3.77 for 0%, 3%, 6% and 9% samples respectively. These values are greater than the reported values in literature for CuO. A shift in the optical and electronic properties can be observed as a function of crystallite size, when sizes of the nano crystallites are smaller than Bohar's excitonic radius (r_b) or comparable to de-Broglie wavelength of charge carriers. This happens as light absorption leads to an electron in conduction band leaving a positive hole in valance band. An expected confinement with the smallness of size occur leading to quantization of energy levels. Thus observed blue shift in the optical absorption spectra with size reduction is a clear indication of energy gap enlargement due to quantum confinement effects **[36, 37]**.

The variation in bandgap of CuO with Zn is not constant and shows an irregular behavior. Initially this value increases with Zn followed by a decrease which increases again marginally. The plots of variation in bandgap (E_g) of CuO with Zn content and grain size are shown in **Fig. 5 (c)**.

Conclusion

We reported that composite hydroxide mediated approach is a feasible route for the synthesis and doping of nanomaterials in single step process. The method was demonstrated for a technologically potential zinc doped copper (II) oxide nanomaterial. The final nanoproduct was a single phase monoclinic structure Cu(II)O with an average grain size in the range of 85.32-124.86 nm and with improved crystalline structure. The nanostructures showed flowers type morphological peculiarities and seem strongly to depend on the Zn concentration. FTIR investigation revealed the characteristic vibrational peaks due to Cu(II)-O bonding. The optical properties demonstrated absorption in the entire UV-vis. region which makes CuO a better alternative candidate for the photovoltaic devices application. The bandgap of pure and

doped Cu(II)O showed an irregular behavior and varies in the range of 3.73 to 3.89 eV. These results demonstrated the feasibility of synthesis of Zn doped CuO nanomaterial by CHM approach with morphological peculiarities and tunable properties. Further investigations are required to realize this approach for the controlled doping and to tune the desired properties of nanomaterial for the high-tech applications. The proposed approach with advantages of rapid synthesis process and high productive ratio will give a potential avenue for further practical scale-up of the production process and applications of novel devices based on doped nanostructures.

Acknowledgements

The authors acknowledge their parent department FUUAST for facilitating in conducting this research work. Further supporting of Quaid-e-Azam University and NUST in characterization is also greatly acknowledged.

Reference

1. Curri, M.L.; Agostiano, A.; Mavelli, F.; Monica, M.D. *Mate. Sci. & Eng. C* **2002**, 22, 423. **DOI:** 10.1016/S0928-4931(02)00191-1
2. Bayansal, F.; Gülen, Y.; Sahin, B.; Kahraman, S.; Cetinkara, H.A. *J. Alloy. Compd*. **2015,** 619, 378. **DOI:** 10.1016/j.jallcom.2014.09.085
3. Armelao, L.; Barreca, D.; Bertapelle, M.; Bottaro, G.; Sada, C.; Tondello, *E. Thin Solid Films* **2003,** 422, 48. **DOI:** 10.1016/S0040-6090(03)00940-4
4. Roh, S.R.; Jung, S.H.; Jeong, S.M.; Kim, S.D. *J. Chem. Technol. Biotechnol.* **2003**, 78, 1104. **DOI:** 10.1002/jctb.910
5. Frietsch, M.; Zuduka, F.; Goschnick, J.; Bruns, M.; *Sens. Actuactors, B, Chem.* **2000**, 65, 339. **DOI:** 10.1016/S0925-4005(99)00353-6
6. Koumoto, K.; Koduka, H.; Seo, W.S.; *J. Mater. Chem*. **2001**, 11, 251. **DOI:** 10.1039/B006850K
7. Jindal, K.; Tomar, M.; Gupta, V.; *Biosens. Bioelectron*. **2012**, 38, 11. **DOI:** 10.1016/j.bios.2012.03.043
8. Sung, W.; Kim, W.; Lee, S.; Lee, H.; Kim, Y.; Park, K.; Lee, S.; *Vacuum* **2007**, 81, 851. **DOI:** 10.1016/j.vacuum.2006.10.002
9. Jariborg, T.; *Physica C* **2007** 454, 5. **DOI:** 10.1016/j.physc.2006.12.019
10. Vidyasagar, C.C.; Naik, Y.A.; Venkatesh, T.G.; *Powder Technol*. **2011,** 214, 337. **DOI:** 10.1016/j.powtec.2011.08.025
11. Yin, Z.; Ding, Y.; Zheng, Q.; Guan, L.; *Electrochemical. Commun*. **2012**, 20, 40. **DOI:** 10.1016/j.elecom.2012.04.005
12. Gao, W.; Yang, S.; Yang, S.; Lv, L.; Du, Y.; *Phy. Lett. A* **2010,** 375, 180. **DOI:** 10.1016/j.physleta.2010.10.065
13. Son, D.I.; You, C.H.; Kim, T.W.; *Appl. Surf. Sci*. **2009** 255, 8794. **DOI:** 10.1016/j.apsusc.2009.06.056
14. Hong, Z.S.; Cao, Y.; Deng, J.F.; *Mater. Lett*. **2002**, 52, 34. **DOI:**10.1016/S0167-577X(01)00361-5
15. Kumar, R.V.; Diamant, Y.; Gedanken, A.; *Chem. Mater*. **2000**, 12, 2301. **DOI:** 10.1021/cm000166z
16. Gurin, V.S.; Alexeenko, A.A.; Zolotovskaya, S.A.; Yumasher, K.V.; *Mater. Sci. Eng. C* **2006**, 26, 952. **DOI:** 10.1016/j.msec.2005.09.021
17. Li, Z.S.; Hui, Z.; Yujie, J.; Deren, Y.; *Nanotechnol*. **2004**, 15, 1428. **DOI:** 10.1088/0957-4484/15/11/007
18. Han, D.; Yang, H.; Zhu, C.; Wang, F.; *Powder Technol*., **2008**, *185*, 286. **DOI:** 10.1016/j.powtec.2007.10.018
19. Wang, W.; Zhan, Y.; Wang, G.; *Chem. Commun*. **2001**, *8*, 727. **DOI:** 10.1039/B008215P
20. Aslani, A.; *Physica B* **2011**, 406, 150. **DOI:** 10.1016/j.physb.2010.10.017
21. Jiang, X.; Herricks, T.; Xia, Y.; *Nano. Lett*. **2002**, 2, 1333. **DOI:** 10.1021/nl0257519
22. Yadav, T.P.; Mukhopadhyay, N.K.; Tiwari, R.S.; *J. Nanosci, Nanotech*. **2007,** 7, 575. **DOI:** 10.1166/jnn.2007.128
23. Khan, T.M.; Zakria, M.; Shakoor, R.I.; Raffi, M.; Ahmad, M.; *Adv. Mater. Lett*. **2015**, 6, 592. **DOI:** 10.5185/amlett.2015.5876
24. Khan, T.M.; Shahid, T.; Zakria, M.; Shakoor, R.I.; *Electron. Mater. Lett.* **2015**, 3, 366. **DOI:** 10.1007/s13391-015-4134-x
25. Hu, C.; Xi, Y.; Liu, H.; Wang, Z.L.; *J. Mater. Chem*. **2009**, 19, 858. **DOI:** 10.1039/B816304A
26. Xu, M.; Wang, F.; Zhao, M.; Yang, S.; Sun, Z.; Song, X.; *Physica E* **2011**, 44, 506. **DOI:** 10.1016/j.physe.2011.09.030
27. Tan, J.; Zhang, W.; Lv, Y.; Xia, A.; *Mate. Res*. **2013,**16, 689. **DOI:** 10.1590/S1516-14392013005000040
28. Fujimura, N.; Nishihara, T.; Goto, S.; Xu, J.; Ito, T.; *J. Cryst. Growth* **1993,** 130, 269. **DOI:** 10.1016/0022-0248(93)90861-P
29. Kuo, T.J.; Huang, M.H.; *J. Phys. Chem*. **2006**, 110, 13717. **DOI:** 10.1021/jp062854x
30. Peng, Q.; Cong, G.W.; Qu, S.C.; Wang, Z.G.; *Nanotechnol*. **2005,** 16, 1469. **DOI:** 10.1088/0957-4484/16/9/008
31. Rahman, A.; Ismail, A.; Jumbianti, D.; Magdalw S.; Sudrajat, H.; *Indo. Chem*. **2009,** 9, 355. **DOI:** 10.14499/ijc-v9i3p355-360
32. Krishnan, S.; Haseeb, A.S.M.A.; Johan, M.R.; *J. Alloy Compd*. **2014**, 586, 360. **DOI:** 10.1016/j.jallcom.2013.10.014
33. Wang, J.; He, S.; Li, Z.; Jing, X.; Zhang, M.; *Colloid Polym. Sci*. **2009,** 287, 853. **DOI:** 10.1007/s00396-009-2040-1
34. Yin, M.; Wu, C.; Lau, Y.; Bruda, C.; Koberstein, J.T.; Zhu, Y.; *J. Am. Chem. Soc*. **2005,** 127, 9506. **DOI:** 10.1021/ja050006u
35. Tsunekawa, S.; Fukuda, T.; Kasuya, A.; *J. App. Phy*. **2000,** 87, 1318. **DOI:** 10.1063/1.372016
36. Dagher, S.; Haik, Y.; Ayesh, A.L.; Tit, N.; *J. Lumin*. **2014,** 15, 1149. **DOI:** 10.1016/j.jlumin.2014.02.015
37. Mohamed, R.M.; Harraz, F.A.; Shawky, A.; *Ceram. Int*. **2014,** 40, 2127. **DOI:** 10.1016/j.ceramint.2013.07.129

